Applications

Christoph Pohl*, Patrick Hegemann, Byungchul An, Markus Grotz and Tamim Asfour

Humanoid robotic system for grasping and manipulation in decontamination tasks

Humanoides Robotersystem für das Greifen und Manipulieren bei Dekontaminierungsaufgaben

https://doi.org/10.1515/auto-2022-0060
Received April 26, 2022; accepted September 17, 2022

Abstract: The disposal of nuclear waste poses a long-standing problem, which has been conventionally handled by human workers. This includes carrying heavy objects, exposure to radiation, and decontamination in full-body protective suits. To improve the working conditions and safety of the workers, robot systems can contribute to tackling some of these problems. So far, most robots in use are manually teleoperated and lack autonomy. To this end, we propose a fully autonomous decontamination setup with the humanoid robot ARMAR-6 [T. Asfour, M. Wächter, L. Kaul, et al., "ARMAR-6: a high-performance humanoid for human-robot collaboration in real world scenarios," *IEEE Robot. Autom. Mag.*, vol. 26, no. 4, pp. 108 – 121, 2019] that can manipulate unknown objects as a first important step of decontamination without the need for human intervention.

Keywords: affordances; decontamination; humanoid robotics; mobile manipulation.

Zusammenfassung: Die Entsorgung nuklearer Abfälle stellt seit langem ein Problem dar, welches üblicherweise von menschlichen Arbeitskräften bewältigt wird. Unter anderem gehören das Tragen schwerer Gegenstände, die Strahlenbelastung und die Dekontamination in Ganzkörperschutzanzügen zu den problematischen Aspekten dieser Arbeit. Um die Arbeitsbedingungen und die Sicherheit der Arbeiter zu verbessern, können Robotersysteme dazu beitragen, einige dieser Probleme zu bewältigen. Bislang werden die meisten Roboter manuell ferngesteuert und können nicht autonom agieren. Daher schlagen wir einen vollständig autonomen Dekontaminationsaufbau mit dem humanoiden Roboter ARMAR-6 [T. Asfour, M. Wächter, L. Kaul, et al., "ARMAR-6: a high-performance humanoid for human-robot collaboration in real world scenarios," *IEEE Robot. Autom. Mag.*, vol. 26, no. 4, pp. 108 – 121, 2019] vor, der unbekannte Objekte als ersten wichtigen Schritt der Dekontamination ohne menschliches Eingreifen manipulieren kann.

Schlagwörter: Affordanzen; Dekontamination; humanoide Roboter; mobile Manipulation.

1 Introduction

The decommissioning of nuclear power plants is a lengthy and expensive process. It involves multiple steps that still need to be handled manually by human workers due to the complex manipulation tasks required to complete them. These tasks are currently performed in inhumane working conditions and require physically straining activities in full-body protective suits. Additionally, the throughput is limited by the time a human worker is allowed to stay in a contaminated area.

Therefore, the automation of the decommissioning process could increase productivity as well as the working conditions and safety of human workers in these inhospitable environments. Furthermore, autonomous or teleoperated manipulation of the objects involved can decrease the cognitive load of the workers. The ability to handle certain parts fully autonomously facilitates a higher throughput, which in turn decreases the cost and duration of the decommissioning process.

On the other hand, the large variety of objects (e.g., size, weight, color, form, texture) which need to be handled

***Corresponding author: Christoph Pohl**, Institute for Anthropomatics and Robotics, Karlsruhe Institute of Technology, Karlsruhe, Germany, e-mail: christoph.pohl@kit.edu
Patrick Hegemann, **Byungchul An**, **Markus Grotz and Tamim Asfour**, Institute for Anthropomatics and Robotics, Karlsruhe Institute of Technology, Karlsruhe, Germany, e-mail: asfour@kit.edu

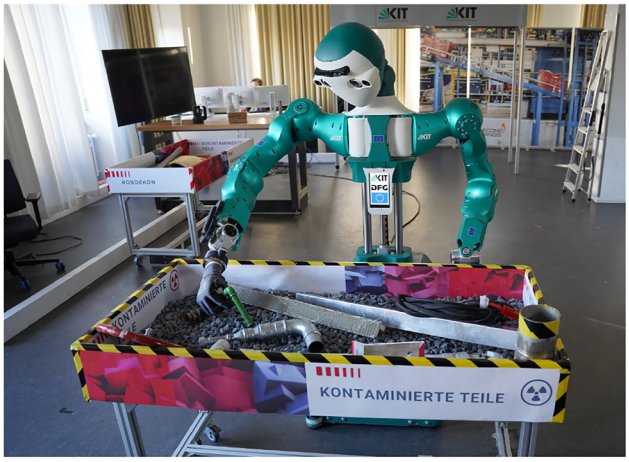

Figure 1: ARMAR-6 grasping an unknown object in a cluttered scenario. This represents the initial state in which dismantled parts of nuclear power plants are delivered to our decommissioning setup.

by a decommissioning system, as well as the uncertainties in the perception and the complex manipulation actions required, complicate the automation process. Therefore, a robot capable of performing these tasks needs to be versatile, precise, and fast. The perception system should be able to handle noise, occlusion, and missing prior knowledge about the objects involved. This is the reason why the automation of the decommissioning process has only progressed slowly. The only robotic applications in the nuclear industry so far are manually teleoperated systems [1], which place a large cognitive load on human operators.

To deal with the aforementioned problems, we present an autonomous decontamination setup, similar to the one displayed in Figure 1, using the humanoid robot ARMAR-6 [2]. Our system is capable of performing complex manipulation actions on unknown objects and can handle all steps of the decontamination process of dismantled nuclear power plant parts – from the delivery of mock-up objects in a box up to the planning and execution of the decontamination trajectories – fully autonomously. This facilitates the removal of human workers from the contaminated zone, while still allowing for intervention in case of errors via teleoperation. Our contributions are (i) a fully autonomous decontamination setup, that can manipulate unknown objects in dynamically changing environments, (ii) continuous monitoring of the process for failures during the execution, and (iii) versatile trajectory planning on the object meshes that are obtained after an autonomous object scanning procedure.

2 Related work

Mobile, ground-based robotic systems have been in use in the nuclear industry and other hazardous environments since the early 1960s [3], where they were mainly used for teleoperated monitoring purposes. Since then, the need for increased safety of human workers, improved working conditions, decreased exposure to radiation, and raised productivity has driven many developments in this area [4].

The use of robots at the nuclear accident in the Fukushima Daiichi nuclear power plants after massive damage due to an earthquake in 2011 can be seen as an example of this technological advance in a real-world emergency scenario. Multiple hurdles, like missing wireless communication, unknown terrain, and high radiation levels, had to be overcome in order to use robots for tasks like debris removal, surveillance, and on-site inspections [5]. As one of the robots used in the field, the efforts of applying the disaster response robot Quince to the Fukushima Daiichi accident are described in [6].

An overview of the challenges and potentials of robotic applications in the nuclear industry is given in [7], while also explaining that mostly manually teleoperated systems are used today. In [8], different software and hardware solutions in the areas of teleoperation, sensing technologies, and autonomous manipulation in decommissioning scenarios are presented. The authors of [1], compare manual teleoperation versus semi-autonomy in a nuclear industry context and highlight that incorporating autonomous robot control techniques can increase the performance in these tasks. Similarly, in our previous work [9], a pilot interface for the teleoperation of a robot in complex manipulation scenarios is developed. Our work described in [10] builds on that and investigates the influence of human decision-making in the grasp selection process on the overall success rate of grasping unknown objects from a box. The results show that the selection of grasp candidates by a human operator increases the success rate to 72% from 57% in the autonomous selection, to 66% in manual teleoperation. However, none of these works provide a solution that can potentially handle all steps of the decontamination process from the delivery of the objects to the actual decontamination.

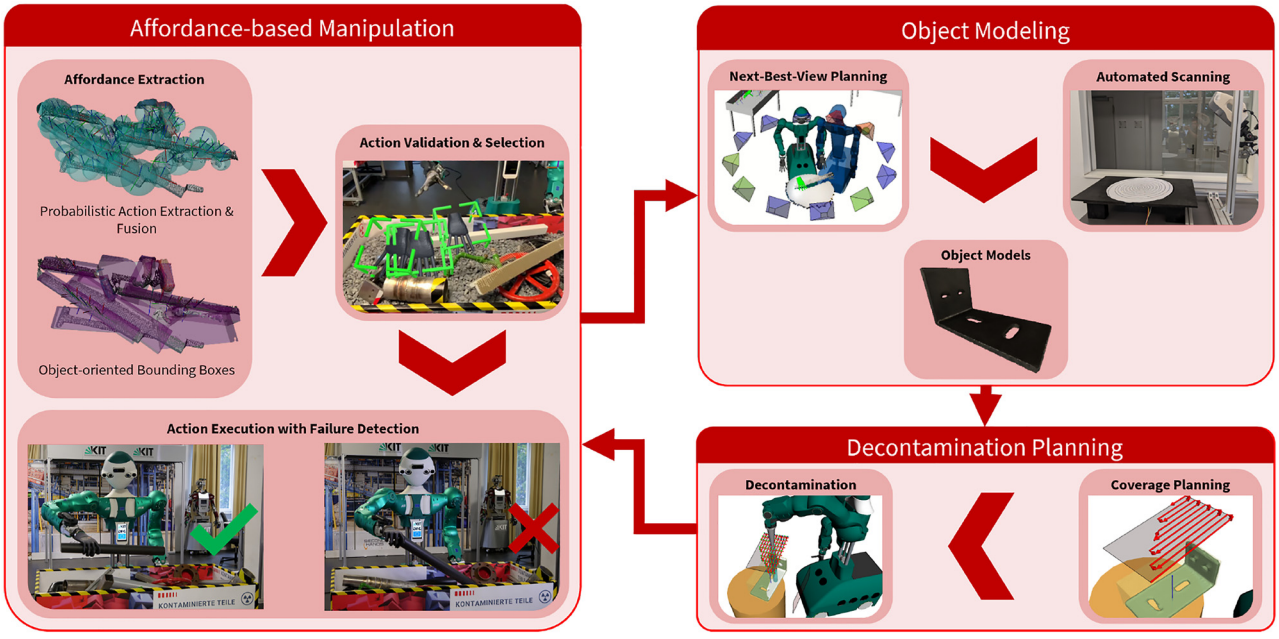

Figure 2: Overview of the autonomous decontamination pipeline presented in this work. The unknown objects are delivered in a box and then grasped and placed on a rotary table. This part is monitored for failures during execution. Afterward, the object is scanned and a trajectory for the decontamination is planned.

3 Autonomous decontamination of unknown objects

In this work, we present a mock-up decontamination cell, that can autonomously process contaminated objects, which usually are cleaned in strenuous manual labor. These objects are comprised of the manually disassembled interior of nuclear power plants, which still have leftover surface radiation and cannot be disposed of in the normal waste cycle. Before these objects are cleared to leave the decommissioning site, they need to be cleaned – usually with high-pressure water or sandblasting – until a certain level of radiation is reached. The dismantled objects are transported in boxes for further cleaning during the decommissioning process. To reproduce the conditions, an automated decommissioning system has to cope with, in as much detail as possible, our mock-up decontamination cell starts with several unknown, featureless objects of different sizes, shapes, and weights in a box.

The cleaning process entails (i) the grasping of an object from the box, (ii) the placement of the object on a rotary table for scanning, and (iii) the autonomous scanning of the object to obtain a precise mesh that can be used for (iv) the subsequent decontamination planning.

An overview of our approach can be seen in Figure 2. For the manipulation of objects in the box, we extract multiple action candidates from perception and autonomously choose a suitable action to execute (Section 3.1). This process is continuously monitored for failures so that a recovery action can be performed if a grasp fails (Section 3.2). Afterward, the object is placed on a table and can be scanned to obtain a detailed object mesh (Section 3.3). Based on these meshes, a coverage planning algorithm is used to compute optimal decontamination trajectories (Section 3.4).

3.1 Affordance-based manipulation of unknown objects

The vision-based manipulation of unknown objects is a complex problem and, therefore, is divided into multiple tasks in the mock-up cell. First, promising manipulation locations in the environment need to be identified. For this, we rely on the concept of affordances [11], which describes interaction possibilities with the environment as properties of objects and was adapted for robotics from cognitive psychology. Afterward, all identified affordances need to be checked for reachability, the preferred hand to use for action execution, and suitable platform placements of the humanoid robot ARMAR-6. A heuristic selection process, which identifies actions with a high success probability, is followed by the compliant execution of the action associated with an affordance. In this way, we can

model actions like grasping, pushing, etc. of objects in the box in the same framework as e.g., the placement of the object on the rotary table.

3.1.1 Affordance discovery

The discovery of affordances in the environment relies only on visual perception and consists of a modular pipeline that receives the raw point clouds from an Azure Kinect RGB-D camera and subsequently extracts action candidates. As the position and dimensions of the box are known, we can incorporate this as prior knowledge and crop the point cloud so that only points inside of the box are considered. Based on this pre-processed point cloud, different approaches for the generation of action candidates can be used to tailor the pipeline to the concrete scenario. In our case, where all objects in the box are unknown we use two different approaches: (I) a grasp and push candidate generation using object-oriented bounding boxes of the objects segmented with a region growing clustering, similar to the approach in [12], and (II) an affordance extraction method based on features of the local surface geometry, combined with a subsequent probabilistic fusion of the action candidates as described in [13].

For the method based on object-oriented bounding boxes (I), the incoming point cloud is first segmented and for each cloud segment, the object-oriented bounding box is calculated. Based on the dimensions of the box, the grasp candidates are aligned with the long side of the box, so that the hand is oriented perpendicular to the box for a top grasp. Push candidates are oriented in a way that the push is executed perpendicular to the long side of the box. This way, multiple action candidates can be extracted for each bounding box by positioning the candidate in intervals along the long side of the box.

In the method based on probabilistic fusion (II), the normals and curvatures of the point cloud are calculated and then clustered into small, spatially coherent surface patches. The averaged geometrical information of each patch is used to heuristically assign affordances to the patch. The associated actions of the patch are fused over multiple observations using *Bayesian Recursive State Estimation* to obtain measures for the accuracy and existence certainty of the affordance.

3.1.2 Validation of affordances and platform placement

Once the concrete action candidates are extracted, they are henceforth treated as generic affordances, independent of the type of action. Before an execution of the actions is possible, a preferred arm of the humanoid robot needs to be chosen. This is done based on the orientation of the action candidate in the plane parallel to the ground, i.e., an arm is chosen so that the orientation of the executing hand is as natural as possible with respect to the torso of the robot. Afterward, the position of the platform is chosen so that the shoulder of the executing arm is on the same *xy*-position as the action candidate. If the *inverse kinematics* (IK) problem is solvable for the TCP of the executing hand at the chosen platform placement, the affordance is declared as reachable and can be selected for execution in the next step. Otherwise, a new robot placement is determined using inverse reachability maps [14].

3.1.3 Autonomous action selection

From all reachable action candidates, one needs to be chosen for execution. The choice depends mainly on the task, i.e., the state of the decontamination process. For retrieving objects from the box, mainly grasp affordances are chosen and only if no feasible grasps are available, a pushing action is executed to change the scene. As we assume that the highest object is easiest to grasp, we choose the highest grasp in the box for execution. To avoid the repeated execution of a grasp that previously led to a failure, all candidates within a small radius of each previously executed grasp are removed from the selection process.

3.1.4 Compliant action execution

The execution of actions is split into four stages itself: (a) positioning of the selected TCP at a pose (called *pre-pose*) directly above the action's pose (called *execution pose*), (b) moving the TCP until contact is detected with the object, (c) executing a unique trajectory associated with an affordance type, and (d) the subsequent retraction of the hand. For the execution of all trajectories, a variable-stiffness impedance controller is used. The stiffness of the controller is chosen empirically for each stage of the execution process and ranges from very stiff and precise at stage (a) to very compliant at stage (c). In stage (a), the chosen TCP is moved to the *pre-pose*, which is the execution pose shifted in positive *z*-direction. This is achieved by moving the TCP along a *Via-Point Movement Primitive* (VMP), see [15], with variable end-pose, which was learned through demonstration by a human operator. We chose VMPs for these motions, as they result in very

Figure 3: A large object being explored by ARMAR-6.

human-like trajectories. Since all stages of the pipeline are supervised by a human operator, this makes it easier to predict the movements of the robot and facilitates an early intervention of the operator in case of potential failures.

From the *pre-pose*, the TCP is compliantly moved to the *execution pose* in stage (b) to prevent damage to the arm, hand, and fingers in case of contact with the environment. In stage (c), a pre-defined hand and finger trajectory is executed for each type of action, e.g., a straight push for the pushing action and a sequential closing of the fingers while lifting the wrist during a grasping action. The stiffness of the controller is chosen dependent on the action. After the action's trajectory has been executed, the hand is lifted to a safe pose above the box in stage (d).

3.2 Continuous failure detection

The execution of pick-and-place tasks is continuously monitored to detect failures, such as failing to lift a grasped object out of the box. In case of a failure, a recovery action is triggered, and the execution is restarted. The failure detection system combines multi-modal sensor data to learn symbolic task models from multiple successful task executions. These learned task models are then used as a reference for detecting failures during the execution of a pick-and-place task.

In the first step of the pipeline, symbolic predicates are extracted from proprioceptive, force, and visual information. The predicates indicate e.g., whether an object is in the hand, or the platform is moving. A decision tree is constructed from these predicates to infer the current robot state depending on the executed action. The sequence of the resulting states and their transitions are then used to build a task graph. In order to learn appropriate task models for failure detection, the task graphs of several executions of the task are recorded. While training the model, a supervisor manually labels the executions as successful or failed. The task model is represented as a Markov chain by calculating the probability of each state transition from the recordings of successful executions. In order to detect failures during the execution, the detected task graph is compared to a learned model of successful executions to determine the failure state. If the current task graph contains unseen transitions, e.g., from having an object in the hand to not having one during grasping, a failure has happened and the recovery action is triggered.

3.3 Object modeling

To plan an optimal decontamination trajectory and monitor its progress, an object model is required. To this end, we automatically create a model of the object from visual perception. For this purpose we apply two strategies, based on the dimensions of the object under consideration:

1. A detailed approach for small objects using an Artec Eva structured light 3D scanner, and
2. A coarser approach for larger objects using the internal RGB-D camera of ARMAR-6.

Once the object is placed on a table, the automated scanning procedure is triggered. First, the dominant plane is detected and removed from the sensor to distinguish the object and supporting surface.

For the detailed approach, the object is rotated using a rotating table. For the coarser approach, the Next-Best-View problem is solved similarly to the methods described in [16]. Here, views are sampled equidistantly around the table with a fixed radius. These views are evaluated using a utility function. Afterward, the visual sensor data stream is aggregated to a single coherent and consistent point cloud. Finally, the object model is created by triangulating sensor measurements. The resulting mesh model is down-sampled for practical reasons. For the detailed approach, a texture is stored in addition to the object model.

Based on the scanned model, a number of auxiliary properties, such as the bounding box and grasp hypotheses, can be generated. The resulting object model and properties are transferred to the long-term memory of the robot, where they can be easily accessed for further processing tasks. Figure 3 shows an example of a large object examined by ARMAR-6. Figure 4 visualizes both external views and object models of several small objects obtained using the detailed approach.

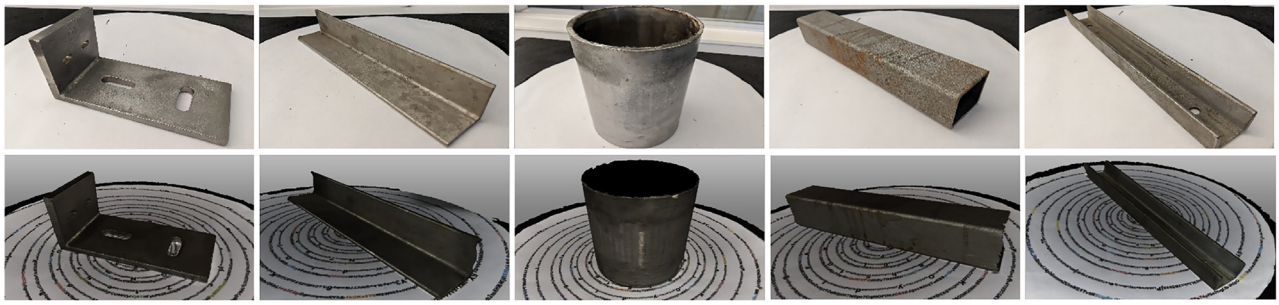

Figure 4: Sample objects scanned with the autonomous scanning setup. The upper row displays the original object on the scanning rig, while the lower row shows the final result (without removal of the plane) of the autonomous scanning procedure for small objects.

3.4 Surface coverage planning

To safely dispose of the objects that are dismantled during the decommissioning process, the residual contamination on the surface must be removed. The goal of the decontamination process is therefore the ablation of the outer surface layer to clean the objects and dispose of them in the normal waste cycle.

The planning of trajectories that cover a maximal part of the contaminated surface with a minimum path length is difficult due to the varying and potentially complex shape of the objects involved. Additionally, the problem is constrained by the kinematic chain of the arm and tool characteristics.

However, solutions to similar problems – like spray painting on regularly parameterized surface patches [17] and the visual inspection with a floating body [18] or a manipulator [19] – exist and can be adapted to the trajectory planning for decontamination. In this work, we simplify the shape of a given object as the optimal object-oriented bounding box. In this way, it is possible to obtain a regular surface for the object, and the coverage planning problem has to be solved only for rectangles. The surface of a rectangle can easily be covered by zigzag path planning with the path interval being determined by the tool model, which, in our case, is approximated by a cone shape for the spraying model.

To plan a joint space trajectory for a robot to follow the path, we first assume that the tool is a floating body and is aligned with the face normal. Nevertheless, possible tool poses reside in a four-dimensional space, resulting in an under-determined IK problem. Therefore, we impose the constraint that the distance between the tool and the target face is fixed. To increase manipulability, the rotation about the tool direction is left variable. It is then possible to use uniform sampling to find the angle about the rotation axis with the largest manipulability.

For the creation of the decontamination path, the target plane is uniformly sampled and the IK is solved for every sample. The angle with the largest linear-velocity manipulability is chosen as the initial orientation for the IK. The sample points are then connected to form a smooth trajectory, while unreachable path segments of the zigzag path are discarded. Finally, the reachable path segments are re-connected.

4 Evaluation

The grasping scenario has been evaluated regarding the quality of the grasp candidate generation in [13] and the accuracy of the failure detection in [20] with multiple real-world experiments on the humanoid robot ARMAR-6. Additionally, we performed multiple simulations to investigate the quality of the planned decontamination trajectories regarding the percentage of the covered surface of the sample objects displayed in Figure 4. A video of the pipeline can be found under https://bit.ly/3djD0vy.

4.1 Grasp candidate extraction

The discovery and extraction of grasp candidates have been extensively tested concerning the two approaches introduced in Section 3.1: (I) the candidate generation based on *Object-Oriented Bounding Boxes* (OOBB) from [12], and (II) the *Probabilistic Action Extraction and Fusion* (PAEF) from [13].

For the comparison of both methods, more than 900 grasp attempts were executed on ARMAR-6. The investigated scenario was designed to show the robustness of the method in a challenging decontamination scenario. To this end, a fixed number of grasp attempts for each approach with a varying number of objects in a box were executed. This was done to investigate the dependency of

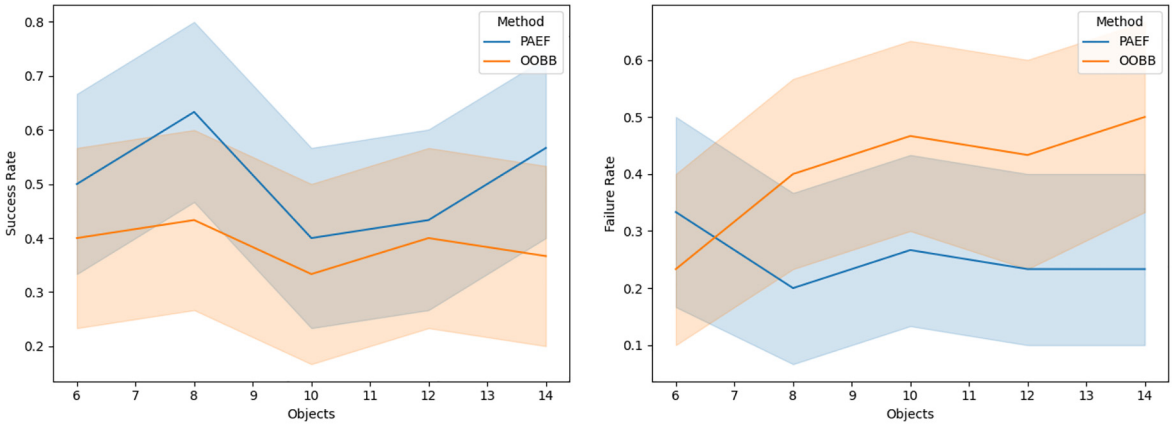

(a) Success Rate **(b)** Failure Rate

Figure 5: Success and failure rates from grasping experiments in [13] with *Object-Oriented Bounding Boxes* [12] and *Probabilistic Action Extraction and Fusion* for a varying number of objects in a box. A grasping attempt was rated as a success if an object was lifted off the ground for more than 5 s and as a failure if the hand collided with another object, or the grasp missed the object entirely. The shaded regions indicate the 95% confidence interval.

grasp candidate generation on the degree of clutter in the scene. The results of each grasp attempt were classified as *grasped*, *stable lifted*, *lifted*, *slipped*, *collision*, or *missed*. The results of the categories *grasped* and *stable lifted* (classified as successful attempts), and *collision* and *missed* (classified as failed attempts) are visualized in Figure 5. From there, it becomes apparent that both methods can robustly deal with a high number of objects. On the other hand, it is visible that the accuracy of the *OOBB* candidates decreases for very cluttered scenes, as the amount of failed grasp attempts increases with a higher number of objects (Pearson's correlation coefficient $\rho_{OOBB} = 0.86$). This can be explained by the strong dependency of the *OOBB* candidates on the segmentation of the scene, which becomes worse for very cluttered scenes. The *PAEF* method can handle this better and the number of failed attempts is independent of the number of objects in the box (Pearson's correlation coefficient $\rho_{PAEF} = -0.52$), as the approach is independent of a scene segmentation to a large degree. The fact that ρ_{PAEF} indicates even a negative correlation stems from the statistically speaking small sample size of 30 grasps per object that were executed. As visible from Figure 5b, the number of failures increases only marginally for more than 8 objects in the box.

4.2 Failure detection

The failure detection system has been evaluated in [20] by conducting over 100 executions of the pick-and-place task. 18 successful executions were recorded in the same scenario for learning the task model prior to the evaluation. Figure 6 shows the results of the evaluation as a confusion matrix of successful and failed executions. Our system is capable of detecting failures in the pick-and-place task with an F_1-score of 0.931. In case of a wrong prediction, it is more often the case that successful executions have been labeled as a failure, than the other way around. This leads to more attempts being necessary to grasp an object, but otherwise has no harmful effects. In case a failed grasp attempt is not recognized, a continued execution could lead to problems for the robot, e.g., when an object is dropped in front of the robot during transportation. In this case, however, a human operator can always intervene in the execution and manually trigger the recovery behavior or even stop the execution.

4.3 Surface coverage planning

To evaluate the surface coverage planning algorithm for the autonomous decontamination of known objects, we conducted experiments in simulation with the scanned objects shown in Figure 4. The evaluation was performed in simulation, as it can directly provide the ground truth surface and the covered surface percentage, which could only be approximated in a real-world evaluation. The experimental setup consists of each object being placed on a turntable in simulation and a stationary robot executing the planned trajectories. The covered surface is calculated by intersecting a cone model (similar to the one used for the trajectory planning) with the mesh of the object and marking the visited surface patches. After the trajectory has been executed, the turntable is rotated by 90°, and

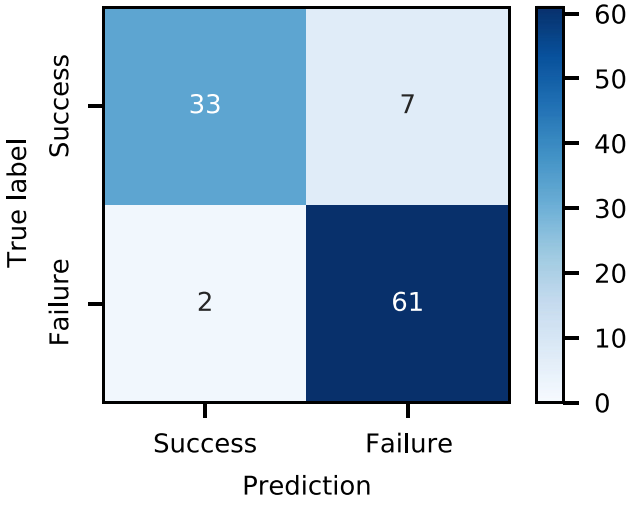

Figure 6: Confusion matrix for the failure detection. The rows represent the true label of an execution, and the columns represent the prediction. Each cell shows the number of corresponding cases.

Table 1: Statistical results of the surface coverage planning. The mean, standard deviation, and maximum values of the covered surface percentage are taken over 10 simulation runs for each of the objects. Each simulation run was started with a different initial angle of the rotary table. Objects are numbered in the order in Figure 4.

Object	1	2	3	4	5
Mean [%]	88.95	94.98	84.50	77.86	88.38
Std [%]	12.42	8.47	8.54	19.66	9.05
Max [%]	98.81	100.00	90.84	99.96	95.91

the coverage planning is repeated. The simulation was run 10 times for each of the scanned objects with different initial turntable angles in the range of $[-\pi, \pi]$. The ratios of covered surface area to total surface area are shown in Table 1. The bottom surface, which is not reachable by the robot since it is facing the table, and the inner surface (e.g., inside the cylinder), which is not scanned during the object modeling phase, are excluded from the evaluation.

The results show that our approach can cover a large percentage of the surface of all objects independent of their shape and size. The relatively high standard deviation shows that the initial pose of the objects and the fixed 90° rotation have a considerable influence on the algorithm. Therefore, finding a suitable initial pose for the objects that takes their shape into account could help to further improve the results. If a mobile robotic system is used for the decontamination, moving the robot to different locations around the object could potentially increase the percentage of reachable end-effector poses. However, to be able to use our approach with simple, stationary manipulators, we did not consider platform movement for the evaluation. Additionally, for a complete decontamination of real objects, it will be important to precisely manipulate the objects so that the inside and bottom surfaces can also be reached by the end-effector for cleaning.

5 Conclusions

In this work, we presented an autonomous approach to the decontamination of unknown objects using the humanoid robot ARMAR-6. Our system can handle all steps from the delivery of the dismantled nuclear power plant parts to the planning and execution of decontamination trajectories without human intervention. This constitutes progress towards the goal of removing human workers from inhospitable or dangerous environments by replacing them with robots that can handle the same tasks (semi-)autonomously.

Different approaches to visual affordance extraction have been presented and compared in extensive real-world experiments. These affordances can be used for the compliant grasping of unknown objects from a box and the subsequent placement on a rotary table. During the execution of manipulation actions, the continuous monitoring of the process allows for the detection of failures and facilitates recovery actions. On the rotary table, the objects can be scanned to obtain the necessary information for the final decontamination. The scanning is performed using an automated scanner setup with a handheld 3D scanner for small objects and a Next-Best-View approach using the internal camera of ARMAR-6. With the geometric information of the object, it is then possible to plan decontamination trajectories for optimal coverage of the object.

In the future, we plan to extend our manipulation pipeline to other scenarios to assess its robustness. Additionally, the real-world decontamination of the scanned objects requires fine-grained manipulation actions, as well as compliant control of the robot arm to cope with the large variety of object shapes and the forces that can arise during surface ablation.

Author contributions: All the authors have accepted responsibility for the entire content of this submitted manuscript and approved submission.
Research funding: The research leading to these results has received funding from the German Federal Ministry of Education and Research (BMBF) under the competence center ROBDEKON (13N14678).

Conflict of interest statement: The authors declare no conflicts of interest regarding this article.

References

[1] N. Marturi, A. Rastegarpanah, C. Takahashi, et al., "Towards advanced robotic manipulation for nuclear decommissioning: a pilot study on tele-operation and autonomy," in *International Conference on Robotics and Automation for Humanitarian Applications (RAHA)*, 2017, pp. 1–8.

[2] T. Asfour, M. Wächter, L. Kaul, et al., "ARMAR-6: a high-performance humanoid for human-robot collaboration in real world scenarios," *IEEE Robot. Autom. Mag.*, vol. 26, no. 4, pp. 108–121, 2019.

[3] I. Tsitsimpelis, C. J. Taylor, B. Lennox, and M. J. Joyce, "A review of ground-based robotic systems for the characterization of nuclear environments," *Prog. Nucl. Energy*, vol. 111, pp. 109–124, 2019.

[4] R. Smith, E. Cucco, and C. Fairbairn, "Robotic Development for the Nuclear Environment: Challenges and Strategy," *Robotics*, vol. 9, no. 4, p. 94, 2020.

[5] R. R. Murphy, S. Tadokoro, and A. Kleiner, "Disaster robotics," in *Springer Handbook of Robotics*, Cham, Springer International Publishing, 2016, pp. 1577–1604.

[6] K. Nagatani, S. Kiribayashi, Y. Okada, et al., "Emergency response to the nuclear accident at the Fukushima Daiichi nuclear power plants using mobile rescue robots," *J. Field Robot.*, vol. 30, no. 1, pp. 44–63, 2013.

[7] D. W. Seward and M. J. Bakari, "The use of robotics and automation in nuclear decommissioning," in *International Symposium on Automation and Robotics in Construction*, Ferrara, International Association for Automation and Robotics in Construction (IAARC), 2005.

[8] I. Vitanov, I. Farkhatdinov, B. Denoun, et al., "A suite of robotic solutions for nuclear waste decommissioning," *Robotics*, vol. 10, no. 4, p. 112, 2021.

[9] P. Kaiser, D. Kanoulas, M. Grotz, et al., "An affordance-based pilot interface for high-level control of humanoid robots in supervised autonomy," in *International Conference on Humanoid Robots*, IEEE-RAS, 2016, pp. 621–628. Available at: KIT-H2T.

[10] C. Pohl, K. Hitzler, R. Grimm, A. Zea, U. D. Hanebeck, and T. Asfour, "Affordance-based grasping and manipulation in real world applications," in *International Conference on Intelligent Robots and Systems*, IEEE/RSJ, 2020, pp. 9569–9576. Available at: KIT-H2T.

[11] J. J. Gibson, "The theory of affordances," in *The Ecological Approach to Visual Perception*, Boston, Houghton Mifflin, 1979, pp. 119–137. chapter 8.

[12] R. Grimm, M. Grotz, S. Ottenhaus, and T. Asfour, "Vision-based robotic pushing and grasping for stone sample collection under computing resource constraints," in *International Conference on Robotics and Automation*, IEEE, 2021, pp. 6498–6504. Available at: KIT-H2T.

[13] C. Pohl and T. Asfour, "Probabilistic spatio-temporal fusion of affordances for grasping and manipulation," *IEEE Rob. Autom. Lett. (RA-L)*, vol. 7, no. 2, pp. 3226–3233, 2022.

[14] N. Vahrenkamp, T. Asfour, and R. Dillmann, "Robot placement based on reachability inversion," in *International Conference on Robotics and Automation*, IEEE, 2013, pp. 1970–1975. Available at: KIT-H2T.

[15] Y. Zhou, J. Gao, and T. Asfour, "Learning via-point movement primitives with inter- and extrapolation capabilities," in *International Conference on Intelligent Robots and Systems*, IEEE/RSJ, 2019, pp. 4301–4308. Available at: KIT-H2T.

[16] M. Grotz, D. Sippel, and T. Asfour, "Active vision for extraction of physically plausible support relations," in *International Conference on Humanoid Robots*, IEEE-RAS, 2019, pp. 463–469. Available at: KIT-H2T.

[17] P. Atkar, H. Choset, and A. Rizzi, "Towards optimal coverage of 2-dimensional surfaces embedded in $\mathbb{R}^3$: choice of start curve," in *IEEE/RSJ International Conference on Intelligent Robots and Systems*, vol. 4, 2003, pp. 3581–3587.

[18] A. Bircher, M. Kamel, K. Alexis, et al., "Three-dimensional coverage path planning via viewpoint resampling and tour optimization for aerial robots," *Aut. Robots*, vol. 40, no. 6, pp. 1059–1078, 2016.

[19] W. Jing, J. Polden, C. F. Goh, M. Rajaraman, W. Lin, and K. Shimada, "Sampling-based coverage motion planning for industrial inspection application with redundant robotic system," in *IEEE/RSJ International Conference on Intelligent Robots and Systems*, IEEE, 2017, pp. 5211–5218.

[20] P. Hegemann, T. Zechmeister, M. Grotz, K. Hitzler, and T. Asfour, "Learning symbolic failure detection for grasping and mobile manipulation tasks," in *International Conference on Intelligent Robots and Systems*, IEEE/RSJ, 2022. Available at: KIT-H2T.

Supplementary Material: The online version of this article offers supplementary material (https://doi.org/10.1515/auto-2022-0060).